Convergence behavior of the random phase approximation renormalized correlation energy

Jefferson E. Bates,* Jonathon Sensenig, and Adrienn Ruzsinszky
Department of Physics, Temple University, Philadelphia, Pennsylvania 19122, USA
(Received 18 March 2017; published 26 May 2017; corrected 25 January 2018)

Based on the random phase approximation (RPA), RPA renormalization [J. E. Bates and F. Furche, J. Chem. Phys. **139**, 171103 (2013)] is a robust many-body perturbation theory that works for molecules and materials because it does not diverge as the Kohn-Sham gap approaches zero. Additionally, RPA renormalization enables the simultaneous calculation of RPA and beyond-RPA correlation energies since the total correlation energy is the sum of a series of independent contributions. The first-order approximation (RPAr1) yields the dominant beyond-RPA contribution to the correlation energy for a given exchange-correlation kernel, but systematically underestimates the total beyond-RPA correction. For both the homogeneous electron gas model and real systems, we demonstrate numerically that RPA renormalization beyond first order converges monotonically to the infinite-order beyond-RPA correlation energy for several model exchange-correlation kernels and that the rate of convergence is principally determined by the choice of the kernel and spin polarization of the ground state. The monotonic convergence is rationalized from an analysis of the RPA renormalized correlation energy corrections, assuming the exchange-correlation kernel and response functions satisfy some reasonable conditions. For spin-unpolarized atoms, molecules, and bulk solids, we find that RPA renormalization is typically converged to 1 meV error or less by fourth order regardless of the band gap or dimensionality. Most spin-polarized systems converge at a slightly slower rate, with errors on the order of 10 meV at fourth order and typically requiring up to sixth order to reach 1 meV error or less. Slowest to converge, however, open-shell atoms present the most challenging case and require many higher orders to converge.

DOI: 10.1103/PhysRevB.95.195158

I. INTRODUCTION

The random phase approximation [1,2] (RPA) is quickly becoming a standard density functional theory [3,4] (DFT) based correlation method for treating weak interactions in both molecular and extended systems. RPA is a nonlocal correlation energy functional that can be naturally combined with a self-interaction free-exchange energy [5,6], correctly describes van der Waals interactions [7–12], and is a parameter-free method that can be used to assess the quality of semilocal DFT [13,14]. Built on top of a semilocal Kohn-Sham reference, RPA has proven to be accurate for thermochemistry and kinetics [13,15], structural properties [16–21], and is typically an improvement over the semilocal functional used to generate the input orbitals [22]. One initial drawback of RPA was its increased computational cost in comparison to semilocal functionals, although many recent implementations have greatly reduced this discrepancy [23–27].

RPA is not a perfect method, however, and suffers from an overestimation of short-ranged correlation and too negative a total correlation energy [1,8,28]. For total energy differences, RPA tends to underbind due to the imperfect cancellation of short-ranged correlation in systems with different numbers of electron pairs [13,15,29–31]. Covalent bond lengths and lattice constants are consistently too large [18–20,32], even if the errors are small. To fix the short-ranged correlation errors of RPA, a correction to the correlation energy beyond RPA (bRPA) is needed and can be obtained from either many-body perturbation theory [33–39] (MBPT) or time-dependent DFT [30,40–45] (TDDFT). In this work we will focus on corrections to RPA from TDDFT due to their efficiency [46] and to demonstrate the behavior of RPA renormalization across the many paradigms of physics and chemistry, from atoms and molecules to periodic solids. The corrections we will explore come through the addition of an exchange-correlation (xc) kernel to the Hartree kernel of RPA when determining the interacting density-density response function.

Kernel corrections to RPA are not without challenges themselves. The exact xc kernel in TDDFT is spatially and temporally nonlocal [47,48], and it satisfies different limits in metallic [49] and insulating [50] systems making it difficult, in theory, to approximate one from the other. Basis set convergence issues are also problematic for adiabatic, semilocal kernels due to the divergence of the on-top pair density [30,42,46]. Certain kernels can also yield electronic instabilities, i.e., imaginary excitation energies, and the simplest examples are the well-known triplet instabilities of time-dependent Hartree-Fock theory [51–54]. While instabilities are somewhat rare for approximate kernels derived from model systems, they can arise for more rigorous kernels such as the frequency-dependent exact-exchange (EXX) kernel [55], even in the electron gas [56]. Avoiding this problem in general is difficult since one cannot predict *a priori* when instabilities will occur for an arbitrary kernel.

One method that ensures a finite correlation energy for kernels with instabilities is RPA renormalization [39], which naturally screens perturbative approximations for the correlation energy through its dependence on RPA as a reference system. The first-order approximation derived from RPA renormalization delivers ∼90% of the total correlation energy for a given kernel [45] and provides a systematic many-body framework for introducing higher-order corrections. Furthermore, RPAr1 was shown in Ref. [56] to explicitly eliminate instabilities in the correlation energy of the electron gas for $r_s > 10$ and N_2 at stretched bond lengths for the EXX

*jeb@temple.edu

kernel. Thus, at least in its first-order approximation, we can *a priori* guarantee the stability of the correlation energy using RPA renormalization with any kernel. For higher orders, it remains an open question as to if or how the instabilities will be reintroduced as one sums the geometric series.

In this work, we explore the convergence behavior of higher-order corrections in the RPA renormalized expansion of the correlation energy beyond first order. Often many-body perturbation theory is taught through the summation of geometric series, though little attention is paid to whether such series summations actually converge. Here, we explore this point explicitly through the direct summation of different finite orders of RPA renormalization and by making comparisons to the full infinite-order results obtained from a traditional beyond-RPA approach. The paper is organized as follows. We first present a brief theoretical background of the adiabatic connection and RPA in Sec. II, and follow with a discussion of a systematic feature of RPA renormalized correlation energy corrections and an overview of the spin dependence in kernel corrected calculations. Results for the homogeneous electron gas are presented in Sec. III, as well as results for a variety of real systems. Several first and second row atoms, open- and closed-shell small molecules, and extended systems including insulators, semiconductors, and metals are all included to demonstrate the robust nature of RPA renormalization. We also highlight the impact that the spin dependence of the kernel and that of the ground state makes on the rate of convergence. Finally, a brief discussion and some conclusions are given in Sec. IV.

II. ACFD-DFT AND RPA RENORMALIZATION

The adiabatic connection (AC) is a useful tool for understanding many exact properties of exchange and correlation in DFT [57–59]. Introducing a coupling constant λ that scales the electron-electron interaction in the many-electron Hamiltonian,

$$\hat{H}_\lambda = \hat{T} + \hat{V}_{\text{ext}} + \lambda \hat{V}_{\text{ee}}, \tag{1}$$

the Hellman-Feynman theorem facilitates the expression of the exchange-correlation energy as an integral over the xc potential contribution [2] as a function of the scaling parameter λ,

$$E_{\text{xc}}[\rho] = \int_0^1 d\lambda\, U_{\text{xc}}[\rho](\lambda). \tag{2}$$

Within the AC framework, the exchange piece is a constant and can be easily separated from correlation. The total energy is computed as $E = E^{\text{EXX}} + E_c$, where

$$E^{\text{EXX}}[\{\phi\}] = T_{\text{s}}[\{\phi\}] + U[\rho] + V_{\text{ext}}[\rho] + E_{\text{x}}^{\text{EXX}}[\{\phi\}] \tag{3}$$

is the Hartree-Fock, or exact-exchange, total energy evaluated using Kohn-Sham (KS) orbitals $\{\phi\}$. T_{s} is the orbital-dependent, single-particle kinetic energy, U is the electronic Hartree repulsion energy, V_{ext} is the single-particle external potential energy which includes electron-nucleus attraction and nuclear-nuclear repulsion energies, and the functional dependence on the orbitals or the density ρ are indicated for each piece. Several formulas exist for computing the explicit exchange energy $E_{\text{x}}^{\text{EXX}}$, e.g., Eqs. (10) and (11) in Ref. [32], with Eq. (10) being the most commonly implemented.

To obtain an expression for the exact correlation energy, the zero-temperature fluctuation dissipation (FD) theorem can be exploited for the correlation potential $U_{\text{c}}(\lambda)$ [2,5,13,60]

$$E_{\text{c}}[\{\phi\}] = -\int_0^1 d\lambda\, \text{Im} \int_0^\infty \frac{d\omega}{2\pi} \langle V[\chi_\lambda(\omega) - \chi_0(\omega)]\rangle, \tag{4}$$

where V is the direct Coulomb (Hartree) interaction, Im indicates the imaginary part, $\langle A\rangle$ is the trace of matrix A, and atomic units are used unless otherwise specified. The density-density response functions χ_λ and χ_0 satisfy the Dyson-type equation

$$\chi_\lambda(x,x';\omega) = \chi_0(x,x';\omega) + \int dx_1 dx_2\, \chi_0(x,x_1;\omega) \times \left[V_\lambda(x_1,x_2) + f_{\text{xc}}^\lambda(x_1,x_2;\omega)\right]\chi_\lambda(x_2,x';\omega), \tag{5}$$

where $x = \{\sigma,\mathbf{r}\}$ is short for the spin and spatial coordinates, $\chi_0(\omega)$ is the KS response function, and $f_{\text{xc}}(\omega)$ is the exact, frequency-dependent exchange-correlation (xc) kernel [48]. The Coulomb interaction is linear in the coupling strength $V_\lambda = \lambda V$, and the behavior of the xc kernel can be determined from uniform coordinate scaling [61]. The KS response function depends on both occupied and unoccupied orbitals, e.g., Eq. (5) in Ref. [62], and therefore the ACFD-DFT constitutes a fifth-rung functional on "Jacob's ladder" of DFT [63].

Once the kernel and the KS response function have been computed, the interacting response function can be extracted from Eq. (5) and the correlation energy from Eq. (4). Under periodic boundary conditions, the Fourier transform of Eq. (4) can be represented as a weighted sum of contributions from wave vectors $\mathbf{q}$ in the first Brillouin zone

$$E_{\text{c}}[\{\phi\}] = -\frac{1}{2\pi}\sum_{\mathbf{q}} \int_0^\infty du \int_0^1 d\lambda \times \text{Re}\,\langle V(\mathbf{q})[\chi_\lambda(\mathbf{q};iu) - \chi_0(\mathbf{q};iu)]\rangle, \tag{6}$$

where the two-point functions V and χ are now replaced by two-index matrices in the reciprocal-lattice vector basis, and the frequency integration has been rotated to the imaginary axis. Unless the spatial frequency or reciprocal-lattice dependence is needed, these indices will be suppressed and are implied from here on. Neglecting the kernel, i.e., $f_{\text{xc}}^\lambda = 0$, defines the RPA response function

$$\hat{\chi}_\lambda = (1 - \chi_0 V_\lambda)^{-1}\chi_0, \tag{7}$$

and the RPA correlation energy via Eq. (4) [2]. Both Eqs. (3) and (4) are typically evaluated non-self-consistently, meaning the set of orbitals $\{\phi\}$ used as input must be generated with a reference exchange-correlation potential, often from a popular generalized gradient approximation (GGA) such as PBE [64] or a meta-GGA such as TPSS [65]. For most systems near equilibrium, this reference determinant dependence is fairly weak from one semilocal functional to another [13,21,39,45,46,66], although using a hybrid functional with a large fraction of exact exchange can negatively impact results from the ACFD-DFT [22].

In order to develop efficient, systematic corrections to RPA from TDDFT, we can recast the Dyson-type equation for

the response function to naturally build in screening from RPA [39]. Using RPA as the reference response function, RPA renormalization (RPAr) refactorizes the Dyson-type equation as

$$\chi_\lambda = \hat{\chi}_\lambda + \hat{\chi}_\lambda f_{\rm xc}^\lambda \chi_\lambda, \tag{8}$$

which is equivalent to solving Eq. (5) if the kernel is included to infinite order, $\chi_\lambda = (1 - \chi_0[V_\lambda + f_{\rm xc}^\lambda])^{-1}\chi_0 = (1 - \hat{\chi}_\lambda f_{\rm xc}^\lambda)^{-1}\hat{\chi}_\lambda$. A key advantage of RPAr, however, is that the KS response function has been eliminated and perturbative expansions of Eq. (8) to include $f_{\rm xc}^\lambda$ will be automatically screened by use of $\hat{\chi}_\lambda$ instead of χ_0. Consequently, RPAr is a robust perturbation theory that avoids the divergence of standard MBPT for zero-gap systems [67,68], in addition to avoiding electronic instabilities that result from having to invert dielectric functions that include $f_{\rm xc}$ [39,56]. Furthermore, this decomposition of the response function results in a total correlation energy that is obtained from a sum of separate terms such that several correlated methods can be computed simultaneously, and the impact of the kernel compared to RPA is easily extracted in a single calculation.

RPAr to first order (RPAr1) was shown to deliver robust results for the electron gas in combination with the EXX kernel [56] and for some simple solids when combined with the non-local energy optimized (NEO) kernel [45]. RPAr has also been applied to molecular systems in combination with the approximate exchange kernel (AXK) yielding a systematic improvement to RPA for a variety of basic chemical processes [39]. Below we explore the impact of corrections beyond first order and discuss the convergence behavior of the RPA renormalized correlation energy corrections.

A. Finite-order RPAr corrections

Traditional literature on MBPT and RPA generally convinces us that by summing up all the terms in a geometric series, one can obtain nonperturbative approximations for quantities such as single-particle self-energies [69] or two-particle response functions [67]. From this standpoint, solution of Eq. (8) would be obtained in an iterative fashion

$$\chi_\lambda^{(0)} = \hat{\chi}_\lambda, \tag{9a}$$

$$\chi_\lambda^{(1)} = \hat{\chi}_\lambda + \hat{\chi}_\lambda f_{\rm xc}^\lambda \hat{\chi}_\lambda, \tag{9b}$$

$$\chi_\lambda^{(2)} = \hat{\chi}_\lambda + \hat{\chi}_\lambda f_{\rm xc}^\lambda \hat{\chi}_\lambda + \hat{\chi}_\lambda f_{\rm xc}^\lambda \hat{\chi}_\lambda f_{\rm xc}^\lambda \hat{\chi}_\lambda, \tag{9c}$$

$$\vdots$$

where the right-hand side is continually plugged into the left-hand side, and the superscript denotes the iteration as well as the order through which the kernel has been included in the response function. Repeating *ad nauseum* leads to the conclusion that this is exactly a geometric series expansion in $\hat{\chi}_\lambda f_{\rm xc}^\lambda$ of the exact solution of Eq. (8), $\chi_\lambda = (1 - \hat{\chi}_\lambda f_{\rm xc}^\lambda)^{-1}\hat{\chi}_\lambda$, just as RPA is a geometric series in the product $\chi_0 V_\lambda$. For this to be true, the sum of finite-order corrections would need to satisfy

$$\sum_{n=0}^{\infty} \left(\hat{\chi}_\lambda f_{\rm xc}^\lambda\right)^n \hat{\chi}_\lambda = \left(1 - \hat{\chi}_\lambda f_{\rm xc}^\lambda\right)^{-1} \hat{\chi}_\lambda, \tag{10}$$

which is challenging to prove in general. Still, we can obtain an nth-order approximation to the infinite-order response function within RPAr by summing corrections from all lower orders

$$\chi_\lambda^{(n)} = \hat{\chi}_\lambda + \sum_{m=1}^{n} \left(\hat{\chi}_\lambda f_{\rm xc}^\lambda\right)^m \hat{\chi}_\lambda. \tag{11}$$

To obtain the total correlation energy, we plug Eq. (11) into Eq. (4) and obtain a series of terms indexed by the number of xc kernels

$$E_c[f_{\rm xc}] = E_c^{\rm RPA} + \Delta E_c^{\rm RPAr1}[f_{\rm xc}] + \Delta E_c^{\rm RPAr2}[f_{\rm xc}] + \cdots, \tag{12}$$

with the RPA correlation energy being the zeroth-order approximation and independent of the choice of xc kernel. The nth-order term for a given kernel can be expressed as

$$\begin{aligned}\Delta E_c^{\text{RPAr-n}}[f_{\rm xc}] &= \int_0^1 d\lambda \int_0^\infty \frac{du}{2\pi}\, \Delta U_{c,\lambda}^{\text{RPAr-n}}[f_{\rm xc}](iu) \\ &= -\int_0^1 d\lambda \int_0^\infty \frac{du}{2\pi} \left\langle V\left[\hat{\chi}_\lambda(iu) f_{\rm xc}^\lambda(iu)\right]^n \right. \\ &\quad \left. \times\, \hat{\chi}_\lambda(iu)\right\rangle \end{aligned} \tag{13}$$

and the total, infinite-order bRPA correction can be computed as [45]

$$\begin{aligned}\Delta E_c^{\rm bRPA}[f_{\rm xc}] &= E_c[f_{\rm xc}] - E_c^{\rm RPA} \\ &= -\int_0^1 d\lambda \int_0^\infty \frac{du}{2\pi} \left\langle V\, \hat{\chi}_\lambda(iu) f_{\rm xc}^\lambda(iu)\, \chi_\lambda(iu)\right\rangle, \end{aligned} \tag{14}$$

using Eqs. (4) and (8). The functional dependence of the bRPA corrections is important to keep in mind since our results indicate that the behavior of the renormalized correlation energy shows some sensitivity to the choice of exchange-correlation kernel, and its accuracy compared to experiment can only be as good as the chosen kernel.

We showed previously that RPAr1 systematically recovers more than 90% of the bRPA correlation energy for the NEO kernel [45], implying that second-order and higher corrections make up the remaining 10%, provided the series expansion converges. RPAr1 also has an analytic λ integral for exchangelike kernels which makes kernel calculations as fast as RPA [39,45]. While we have not been able to analytically prove the convergence of the RPAr series, we demonstrate numerically that it does tend to converge to the infinite-order result in both model and real solids, as well as for finite systems. This is remarkable for a series expansion of the correlation energy since traditional MBPT perturbation expansions based on noninteracting references are not guaranteed to converge at higher orders and the convergence is not necessarily monotonic [70–73]. Further tests are required to see if this behavior also holds for systems with explicit instabilities, such as using the EXX kernel in the electron gas [56]. As an added bonus, the convergence of RPAr is found to be monotonic from below for the total correlation energy because each correction is positive and, in practice, smaller than the previous order.

B. Positivity of RPAr corrections

The sign of each correction can be understood from the properties of the trace, if the matrix representations of the response functions and xc kernel satisfy some reasonable conditions. The even and odd orders of RPA renormalization have slightly different structures, so we will focus on the first- and second-order RPAr corrections as examples, with generalizations to higher orders being straightforward. To show the signed character of the corrections, it is sufficient to analyze the correlation potential contributions from each order of RPAr from Eq. (13) at full coupling and fixed frequency because if the integrand is non-negative, so are the integrals. For the following analysis to hold, the matrix representations of the Coulomb interaction, the xc kernel, and the response function must be Hermitian and positive-definite, negative-definite, and negative-definite, respectively. If one of these conditions is not satisfied, then the following analysis may not hold, but in practice we have not found a case where any order of a beyond-RPA correction is negative within RPA renormalization.

Factorizing the Coulomb interaction as $V = V^{\frac{1}{2}}V^{\frac{1}{2}}$ and using the cyclic invariance of the trace, the RPAr1 correction can be brought to a symmetric form

$$\Delta U_c^{\mathrm{RPAr1}}[f_{\mathrm{xc}}] = -\langle V\hat{\chi}\, f_{\mathrm{xc}}\hat{\chi}\rangle = -\langle V^{\frac{1}{2}}\hat{\chi}\, f_{\mathrm{xc}}\hat{\chi}\, V^{\frac{1}{2}}\rangle. \quad (15)$$

Since f_{xc} is Hermitian negative-definite, its square root is anti-Hermitian [74], and the quantity inside of the trace can be factorized to a quadratic form

$$\begin{aligned} -\langle V^{\frac{1}{2}}\hat{\chi}\, f_{\mathrm{xc}}\hat{\chi}\, V^{\frac{1}{2}}\rangle &= -\langle [V^{\frac{1}{2}}\hat{\chi}(f_{\mathrm{xc}})^{\frac{1}{2}}][(f_{\mathrm{xc}})^{\frac{1}{2}}\hat{\chi}\, V^{\frac{1}{2}}]\rangle \\ &= -\langle [V^{\frac{1}{2}}\hat{\chi}\, f_{\mathrm{xc}}^{\frac{1}{2}}][V^{\frac{1}{2}}\hat{\chi}(-f_{\mathrm{xc}}^{\frac{1}{2}})]^{\dagger}\rangle \\ &= \langle [V^{\frac{1}{2}}\hat{\chi}\, f_{\mathrm{xc}}^{\frac{1}{2}}][V^{\frac{1}{2}}\hat{\chi}\, f_{\mathrm{xc}}^{\frac{1}{2}}]^{\dagger}\rangle. \end{aligned} \quad (16)$$

Equation (16) has the form $\langle AA^{\dagger}\rangle$, therefore, the trace is guaranteed to be non-negative, and we have that the first-order RPA renormalized correction is a positive correction to RPA. For any odd order $n = (2m+1)$, for $m = 0,1,2,\ldots$, the same analysis gives the following general form:

$$\begin{aligned} \Delta U_c^{\mathrm{RPAr\text{-}(2m+1)}}[f_{\mathrm{xc}}] = \langle &[V^{\frac{1}{2}}\hat{\chi}(f_{\mathrm{xc}}\hat{\chi})^m(f_{\mathrm{xc}})^{\frac{1}{2}}] \\ &\times [V^{\frac{1}{2}}\hat{\chi}(f_{\mathrm{xc}}\hat{\chi})^m(f_{\mathrm{xc}})^{\frac{1}{2}}]^{\dagger}\rangle. \end{aligned} \quad (17)$$

For the even orders of RPAr corrections, we can start with the second-order term and make similar rearrangements except that the RPA response function should be positioned in the center of the trace

$$\begin{aligned} U_c^{\mathrm{RPAr2}}[f_{\mathrm{xc}}] &= -\langle V^{\frac{1}{2}}\hat{\chi}\, f_{\mathrm{xc}}\hat{\chi}\, f_{\mathrm{xc}}\hat{\chi}\, V^{\frac{1}{2}}\rangle \\ &= \langle [V^{\frac{1}{2}}\hat{\chi}\, f_{\mathrm{xc}}\hat{\chi}^{\frac{1}{2}}][V^{\frac{1}{2}}\hat{\chi}\, f_{\mathrm{xc}}\hat{\chi}^{\frac{1}{2}}]^{\dagger}\rangle. \end{aligned} \quad (18)$$

Instead of factorizing the kernel, the even orders require one to factorize the RPA response function and the explicit negative sign from the definition of the ACFD correlation potential also drops out, leaving a non-negative trace. The general form for any even order $n = 2m$ for $m = 1,2,3,\ldots$ follows from Eq. (13):

$$U_c^{\mathrm{RPAr\text{-}(2m)}}[f_{\mathrm{xc}}] = \langle [V^{\frac{1}{2}}(\hat{\chi}\, f_{\mathrm{xc}})^m(\hat{\chi})^{\frac{1}{2}}][V^{\frac{1}{2}}(\hat{\chi}\, f_{\mathrm{xc}})^m(\hat{\chi})^{\frac{1}{2}}]^{\dagger}\rangle, \quad (19)$$

and thus *any order* correction to RPA computed from RPA renormalization will be a positive correction. Although this analysis does not give any information about the relative sizes of each order, which would be required to prove convergence of the series, it does establish that the monotonic convergence we observe in our numerical calculations has an analytical origin.

This analysis also establishes the systematic nature of the resummations carried out using RPA renormalization in comparison to traditional MBPT. If the KS response function is used to compute perturbative corrections to RPA, mixed terms that contain different powers of V and f_{xc} will arise, and these terms do not all have the same signed contribution to the correlation energy. For instance, one of the second-order MBPT contributions to the response function is $\chi_0 V_\lambda \chi_0 f_{\mathrm{xc}}^\lambda \chi_0$, which leads to the following correlation-potential contribution:

$$\Delta U_{c,\lambda}^{(2)}[f_{\mathrm{xc}}] \propto -\langle V\chi_0 V_\lambda \chi_0 f_{\mathrm{xc}}^\lambda \chi_0\rangle. \quad (20)$$

We can manipulate this trace to a quadratic form

$$\begin{aligned} &-\langle V\chi_0 V_\lambda \chi_0 f_{\mathrm{xc}}^\lambda \chi_0\rangle \\ &\quad = -\lambda\langle \chi_0^{\frac{1}{2}} V\chi_0 f_{\mathrm{xc}}^\lambda \chi_0 V\chi_0^{\frac{1}{2}}\rangle \\ &\quad = -\lambda\langle [\chi_0^{\frac{1}{2}} V\chi_0 f_{\mathrm{xc},\lambda}^{\frac{1}{2}}][(-\chi_0^{\frac{1}{2}})V\chi_0(-f_{\mathrm{xc},\lambda}^{\frac{1}{2}})]^{\dagger}\rangle \\ &\quad = -\lambda\langle [\chi_0^{\frac{1}{2}} V\chi_0 f_{\mathrm{xc},\lambda}^{\frac{1}{2}}][\chi_0^{\frac{1}{2}} V\chi_0 f_{\mathrm{xc},\lambda}^{\frac{1}{2}}]^{\dagger}\rangle, \end{aligned} \quad (21)$$

and find that the resulting contribution to the correlation energy will be negative since the trace and λ are both positive. There are infinitely many of these cross terms that arise in traditional MBPT due to the expansion of the inverse $[1-\chi_0(V+f_{\mathrm{xc}})]^{-1}$, and including them in an unbalanced way could lead to oscillations in the summation of perturbative contributions to the correlation energy. Thus, without any information on the relative contribution of each order in traditional MBPT, it is difficult to know if the sum of many corrections will have a fixed sign [71,75]. RPA renormalization eliminates this challenge, however, as it exactly includes sums over specific subsets of these mixed terms [39]. In fact, the resummations of RPA renormalization to nth order in the response function are characterized as the exact sum of contributions from traditional MBPT containing any number of V interactions and only n f_{xc} interactions. Consequently, as the analysis above demonstrates, this translates into all possible RPA renormalized contributions having the same sign.

C. Spin dependence of the kernel and RPAr

Thus far, we have not been explicit with the spin dependence of the kernel or the response functions. For RPA, the spin dependence is unimportant because the Coulomb kernel is identical for each block of the 2×2 matrix equation, and so rather than deal with separate spins, the spin-summed response function can be directly computed and the correlation energy extracted analogously to the spin-unpolarized case [46]. This simplification also applies for xc kernels that do not have spin-dependent forms and depend only on the total density. For spin-polarized systems and kernels that depend explicitly on spin, however, the Dyson equation becomes a 2×2 matrix equation in spin space that cannot be reduced in dimensionality. Kernels

derived from MBPT tend to incorporate spin dependence naturally, but building in spin dependence for model electron gas kernels is more challenging.

For exchangelike kernels, an exact constraint on the spin scaling of the kernel is inherited from the spin scaling of the exchange energy in DFT [46]:

$$f_{\mathrm{x},\sigma\sigma'}[\rho_\alpha,\rho_\beta] = 2\, f_{\mathrm{x}}[2\rho_\sigma]\,\delta_{\sigma\sigma'}. \tag{22}$$

This constraint is automatically satisfied by kernels such as NEO, AXK, or the EXX kernel [56,76], however, building this feature into other model kernels is less straightforward. In the construction of the spatially renormalized adiabatic DFT kernels of Olsen and Thygesen, rALDA [42,46] and rAPBE [44], the authors have relaxed this constraint and instead use a spin-dependent kernel which satisfies the following condition for spin-unpolarized systems:

$$\frac{1}{4}\sum_{\sigma\sigma'} f_{\mathrm{x},\sigma\sigma'}[\rho/2,\rho/2] = f_{\mathrm{xc}}[\rho]. \tag{23}$$

In conjunction with their kernel construction procedure, this constraint ensures that some of the basis set convergence issues that affect the adiabatic LDA (ALDA) kernel are eliminated [30,46]. Olsen and Thygesen have demonstrated and discussed that the spin-polarized forms of rALDA and rAPBE deliver improved atomization and cohesive energies compared to the spin-independent form, which is a key advantage for choosing these kernels in practical applications to materials such as metal oxides [77]. The simplest demonstration of the effect was also illustrated in Ref. [21] for the atomization of H_2 where using the spin-dependent kernel increases the atomization energy by 0.5 eV compared to the spin-independent kernel, resulting in substantially better agreement with experiment. The impact the spin dependence of the kernel has on the convergence of RPA renormalization is not necessarily obvious. We explore this issue below by comparing the convergence of spin-dependent and -independent forms of the rAPBE kernel for several spin-polarized atoms and small molecules, the ferromagnetic bcc phase of iron and (0001) surface of cobalt, and the antiferromagnetic ground state of rocksalt NiO [78].

D. Computational details

Using a modified version of the GPAW code [79–81], we have implemented RPA renormalization to arbitrary order in conjunction with the spin-dependent (rADFT) and spin-independent (rADFTns) forms of the exchangelike kernels rALDA and rAPBE, as well as the spin-independent, static exchange-correlation kernel CP07 [41]. When necessary we use the notation RPAr@kernel to denote which kernel has been used with RPA renormalization. The rALDA and rAPBE kernels have been demonstrated to improve upon RPA for energy differences and structural properties, and preserve the accurate description of dispersion interactions for atoms, molecules, and solids [19,42,44,46,77]. The static CP07 [41] xc kernel yields accurate structural properties for bulk solids [19], but its impact on energy differences within the ACFD-DFT remains unexplored.

In addition to specifying the kernel within GPAW, one must specify an averaging scheme to compute the kernel in the reciprocal-lattice basis since there are multiple ways to extend homogeneous electron gas kernels to inhomogeneous systems [19,42,43,82]. We have implemented RPAr to be compatible with both the density and wave-vector averaging schemes, though we have used wave-vector symmetrization throughout to ensure that the kernel is symmetric in the reciprocal-lattice basis because of its computational advantages, as discussed in Ref. [19]. There is the added bonus that the wave-vector symmetrization also preserves the proper divergence behaviors for the "head" and "wings" of the kernel in the $q \to 0$ limit [19]. We checked that for MgO the convergence behavior was analogous with either wave-vector or density-based averaging (see Table S1 in the Supplemental Material [83]), although the magnitudes of the correlation energies differ by a few percent [19]. For a concise and informative comparison of the various electron-gas model kernels and kernel-averaging schemes, see Ref. [19] and references therein. Calculations were performed within the projector-augmented wave formalism [84] using the 0.9.20000 GPAW data sets, which treat the $4s$ and $3d$ shells as a part of the valence for transition-metal atoms, as well as treating the $3p$ semicore states for Ni [21].

Results for real systems were obtained using PBE orbitals to construct the Kohn-Sham reference determinant, and gamma-centered Monkhorst-Pack k-point meshes [85] were used throughout. The maximum cutoff for the response function was chosen between 300 and 400 eV, the number of bands was chosen to be equal to the number of plane waves, and the perturbative approach from Ref. [86] was used to treat the divergence of the Coulomb interaction at small wave vectors. The frequency integral was performed as in Ref. [62] using a 16-point Gauss-Legendre quadrature, and with a frequency scale of 2 for nonmetals, and 2.5 for metals [31]. Extrapolation of the correlation energies to the basis set limit were performed using the Harl-Kresse [62] method with at least four cutoffs below the maximum. The cutoff used to generate the wave functions for the response function was 600 eV. Fermi-Dirac occupations corresponding to an electronic temperature of 0.01 eV were used for all periodic systems. A Wigner-Seitz truncation scheme [87] was used to treat the small wave-vector divergence of the Coulomb interaction in the exchange energy.

For atomic and molecular systems, we used rectangular boxes with unequal side lengths to break spatial symmetry, and extrapolated the correlation energy from calculations at plane-wave cutoffs of 250 and 300 eV for the response function. These cutoffs were previously shown to deliver small errors compared to extrapolations with higher cutoffs for RPA [31]. Larger plane-wave cutoffs, box sizes, or volume-based extrapolations of the correlation energy [62] would be needed to obtain fully converged results for each kernel, however, the relative performance of RPAr to the infinite-order method is usually independent of the basis for cutoffs larger than 250 eV. For atoms, a larger variation in finite cutoff and extrapolated values can result in slower convergence of RPAr for the extrapolated results. For molecules and bulk systems, the differences between finite cutoff and extrapolated results tends to be negligible for any k mesh and cutoffs above 200 eV. The computational settings needed to reproduce our results have been included in Table S2 in the Supplemental Material [83].

Results for the electron gas were obtained using an in-house PYTHON code. Gauss-Legendre quadratures of 12–20 points were used for the frequency and coupling-strength

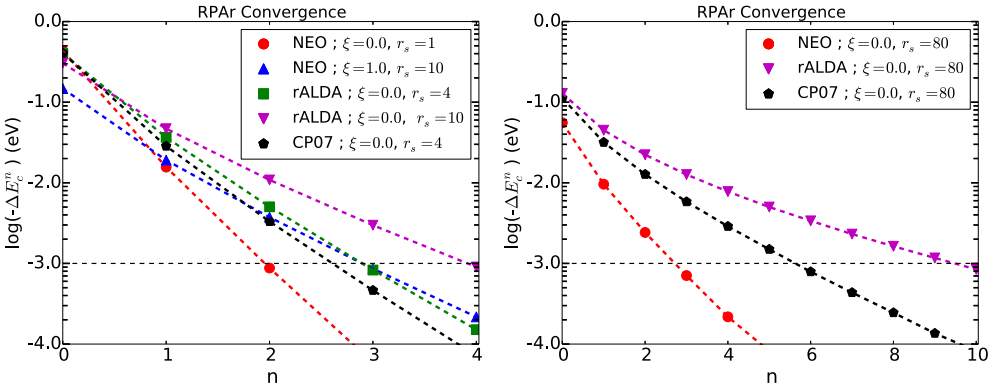

FIG. 1. Convergence of RPA renormalization to the infinite-order correlation energy for selected densities of the electron gas of spin polarization ξ with the NEO, rALDA, and CP07 kernels. $\Delta E_c^n = \sum_i^n \Delta E_c^{\text{RPAr-}i} - \Delta E_c^{\text{bRPAr}}$ is the error for a given order n of RPA renormalization in comparison to the infinite-order result. The dashed line corresponds to 1 meV error. For typical densities between $r_s = 1$ and 10, RPAr converges to meV accuracy between second and fourth order for each kernel. As the density decreases, the convergence slows, and at very low densities (large r_s) the form the xc kernel makes a noticeable impact on the number of orders needed to reach convergence.

integration, while the q integration is implemented using the rectangle method over $0 < q \leqslant 15$ a.u. with 3000 points. The exchangelike NEO kernel [45] and the static CP07 exchange-correlation kernel [41] excluding the $q \to \infty$ limit were also implemented in conjunction with RPAr for the electron gas. We also note that for the electron gas that rALDA and rAPBE are equivalent [77].

Before discussing the results, we would like to emphasize a few aspects of the computational costs associated with finite-order RPAr. As mentioned above, RPAr1 has an analytic λ integral for exchangelike kernels without spin dependence, which means that a savings of N_λ is theoretically achieved for the correlation energy calculation. Given χ_0 the calculation of the correlation energy typically scales as N^3, where N is a measure of system size. The analytic integral does not reduce the total cost by a factor of N_λ since the construction of χ_0 scales as N^4, but in practice reduces the cost by a factor of between 2 and 3 in comparison to the infinite-order method. Higher orders than RPAr1 do not result in any formal savings compared to the infinite-order method since a numerical integration over λ is required in both cases. Furthermore, our brute-force implementation relies on repeated matrix-matrix multiplications which add to the overhead and increase the cost of finite-order RPAr beyond that of the infinite-order approach. Still, for the first few orders, the difference in cost is marginal, with the added benefit that RPA and beyond-RPA results are available from a single calculation.

III. RESULTS

First, we present the convergence behavior of RPA renormalization for the electron gas and follow with real systems. We demonstrate the rapid convergence for RPAr when spin-independent kernels are used to compute the correlation energy and highlight the challenges associated with the spin-dependent kernel that we tested. To demonstrate the robust character of the RPAr expansion, we have included results for the first-row, open-shell $2p$ elements and Mg, small molecules such as N_2, CO, and O_2 ($\mu_B = 2$), and extended systems that are insulators (MgO, NiO), semiconductors (C, Si), and metals (Fe, Rh, Al, Co). We utilize log plots to analyze the convergence of the RPAr series, Eq. (11), with the conventions that

$$E_c^{\text{RPAr-}n}[f_{\text{xc}}] = E_c^{\text{RPA}} + \sum_{m=1}^{n} \Delta E_c^{\text{RPAr-}m}[f_{\text{xc}}], \tag{24}$$

and the error of a given order

$$\Delta E_c^n[f_{\text{xc}}] = \sum_{m=1}^{n} \Delta E_c^{\text{RPAr-}m}[f_{\text{xc}}] - \Delta E_c^{\text{bRPA}}[f_{\text{xc}}] \tag{25}$$

is the difference between beyond-RPA contributions for a given kernel since the RPA part drops out. Note that the value at $n = 0$ in these plots is the log of the total beyond-RPA correction, Eq. (14), by construction.

A. Electron gas and RPAr convergence

Figure 1 demonstrates the convergence of the correlation energy per particle for the RPAr series evaluated with the NEO kernel for both spin-unpolarized and fully polarized limits of the homogeneous electron gas (HEG) at selected densities. The convergence of the rALDA and CP07 kernels is also shown for the spin-unpolarized case. We will use the notation RPAr@kernel to indicate which kernel was used to evaluate the bRPA correlation energy when needed. Numerical values for each kernel are reported in the Supplemental Material [83]. RPAr evaluated with each kernel converges rapidly to the infinite-order result reaching better than 1 meV accuracy between second and fourth order for r_s between 1 and 10. This is direct evidence that the short-ranged forces in the HEG can in fact be accounted for with a relatively low-order expansion in the product $\hat{\chi} f_{\text{xc}}$ for a wide range of densities. For RPAr@NEO, the convergence is fast for both spin-unpolarized and fully polarized regimes, but as the density decreases so does the convergence rate. This is expected since exchange-correlation effects are expected to be more important for spin-polarized systems and in the low-density limit. The inclusion of f_{xc} to higher orders is therefore needed as the density decreases in order to recover the infinite-order result. Even still, the RPAr series is converged to less than 1 meV error

TABLE I. Beyond-RPA correlation energies (meV/per particle) for the HEG from the infinite-order method [Eq. (14)] with the NEO, rALDA, and CP07 kernels. The exact results were obtained by subtracting RPA from the PW92 correlation energy for a given r_s. NEO is accurate for small r_s where it is exact to second order, but becomes an underestimate as r_s increases, while rALDA and CP07 remain accurate over a wide range of r_s. RPA renormalization is limited in accuracy by the infinite-order method compared to exact references as discussed in Ref. [45].

r_s	NEO	rALDA	CP07	Exact
1	435	539	357	517
4	283	404	301	406
10	188	305	244	329
80	56	128	112	154

by second order for $r_s = 1$ and by fourth order for $r_s = 10$ for all three kernels.

As the density becomes exceptionally low, the impact that the form of the xc kernel has on the convergence of RPAr becomes more apparent. Although NEO, rALDA, and CP07 all yield similar convergence rates for $r_s < 10$, at $r_s = 80$ the rALDA kernel converges much more slowly than the other two, requiring terms up to 10th order to reach less than 1 meV error. In contrast, the CP07 kernel requires six orders to reach the same accuracy and the NEO kernel only three. NEO and rALDA both scale linearly with λ, so the difference in their convergence behaviors must stem from the actual functional form of $f_x(\mathbf{q})$, where the former is based on a Gaussian form and the latter is a combination of step functions. NEO and CP07 are actually quite similar in their functional form, except that CP07 scales nonlinearly with λ, which could be the origin of the slower convergence for CP07 compared to NEO. The slower convergence of rAPBE compared to CP07 is not limited to the electron gas, and persists for the spin-unpolarized physical systems we tested.

For completeness, we report the spin-unpolarized, infinite-order bRPA correlation energies for NEO, rALDA, and CP07 in Table I. The exact values were obtained by subtracting RPA from the PW92 correlation energies. As discussed in Refs. [41,42,45] the performance of each kernel varies with r_s. NEO is exact in the high-density limit since it was energy optimized to yield the second-order exchange contribution to the correlation energy of the HEG [45,88], while the static CP07 was parametrized to two sum rules of the HEG [41]. rALDA also satisfies one of those sum rules related to the $q \to 0$ limit of the exact HEG kernel, but with a linear scaling in λ unlike the nonlinear scaling of CP07 [42]. NEO and CP07 are systematic underestimates for all r_s, while rALDA overestimates bRPA correlation in the high-density limit and underestimates at lower densities. Since RPA renormalization at low order systematically underestimates the infinite-order correction, the accuracy of finite-order RPAr in comparison to an exact reference is bounded by that of the infinite-order result. We reiterate the point made in Ref. [45] that for kernels with infinite-order results that overestimate the bRPA correction, RPA renormalization tends to reduce the error compared to the reference, e.g., rALDA for small r_s. However, for kernels with infinite-order results that underestimate a reference bRPA correction, RPAr tends to further increase the error, e.g., the NEO kernel for moderate to large r_s.

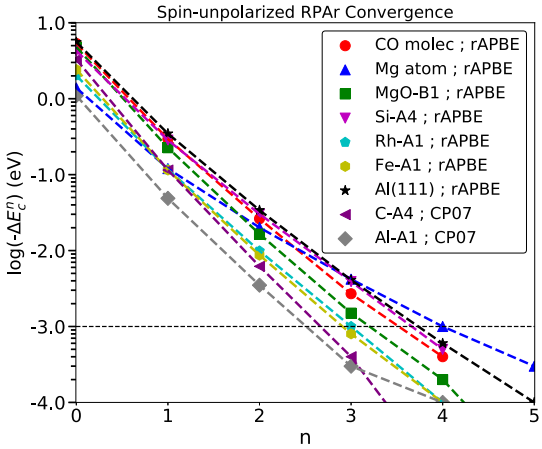

FIG. 2. Convergence of RPA renormalization for real systems near their equilibrium geometries using the rAPBE and CP07 kernels. For spin-unpolarized systems, convergence to the infinite-order result is fast and largely independent of the details of the system such as band gap or dimensionality. For an atom, a molecule, several semiconductors, an insulator, three bulk metals, and one metallic surface, RPAr is converged to less than 1 meV error by fourth order.

B. RPAr convergence for physical systems

For the spin-unpolarized physical systems that we chose, Fig. 2 illustrates that the convergence of RPAr is still fast and analogous to the HEG. Although we have focused on the rAPBE kernel, RPAr works equally well for rALDA (see Table II for a comparison for silicon), and we assume the conclusions based on rAPBE for other systems apply equally to both kernels. Less than 5 meV error is reached for these systems at third order and adding the fourth-order correction reduces the error to less than 1 meV. What is most remarkable about the convergence behavior is that it is independent of the nature of the KS-orbital spectrum. The convergence is smooth and rapid for everything from atomic magnesium or

TABLE II. Comparison of RPAr convergence using rALDA and rAPBE for diamond silicon with respect to the order of the expansion n. LDA input orbitals were used to compute the rALDA kernel results, while PBE input orbitals were used for rAPBE. RPAr converges rapidly to the infinite-order result [Eq. (14)] with both kernels, the error dropping below 1 meV by fourth order.

(eV/Si_2)	rALDA		rAPBE	
n	$E_c^{\text{RPAr-}n}$	$\Delta E_c^{\text{RPAr-}n}$	$E_c^{\text{RPAr-}n}$	$\Delta E_c^{\text{RPAr-}n}$
0 (RPA)	–12.1975	0.0000	–12.1344	0.0000
1	–8.6049	3.5926	–8.1521	3.9823
2	–8.4141	0.1908	–7.8980	0.2541
3	–8.3977	0.0164	–7.8716	0.0264
4	–8.3960	0.0017	–7.8682	0.0034
5	–8.3958	0.0002	–7.8677	0.0005
∞	–8.3958	3.8017	–7.8677	4.2667

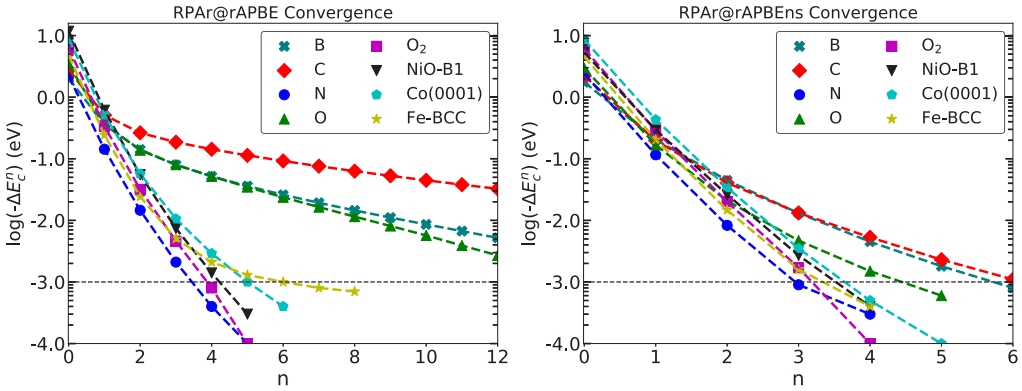

FIG. 3. Convergence of RPA renormalization using the spin-dependent (left) and spin-independent (right) rAPBE kernel for several first-row atoms with unpaired electrons, oxygen molecule ($\mu_B = 2$), and ferromagnetic iron in the bcc phase and the Co(0001) surface. For B, C, and O, the convergence of RPA renormalization is extremely slow when combined with the spin-dependent kernel. For the spin-independent rAPBEns kernel, all systems converge much more rapidly, although B, C, and O still converge more slowly than the other examples. Other than the open-shell atoms, the convergence of rAPBE and rAPBEns are similar, highlighting a unique challenge of RPAr combined with these kernels for atomic systems.

molecular carbon monoxide to the three major paradigms of bulk materials: metals [Fe-fcc, Rh-fcc, Al-fcc, and Al(111)], semiconductors (diamond C and Si), and insulators (MgO). This independence of the KS gap stems directly from the replacement of the reference response function χ_0 with $\hat{\chi}$, and the renormalization of the KS excitations to their RPA counterparts when computing the xc-kernel corrections. Spin-polarized systems prove to be more challenging, however, and the convergence of RPA renormalization can be hampered by the functional form of the kernel.

Figure 3 illustrates the difficulties that an expansion such as Eq. (12) can potentially encounter and reinforces the functional dependence of beyond-RPA correlation within RPA renormalization. It is worth emphasizing that the extremely slow convergence of RPA renormalization for some spin-polarized atomic systems seems to be the exception rather than the norm, with molecular or extended systems of any spin polarization all converging at similar rates with the same kernel. The strength of short-ranged interactions in atomic systems has always been a challenge for many electronic structure methods, being largely responsible for the difficulty in predicting accurate total atomization energies [89]. The additional electrostatic attraction provided by other atoms in a molecule or by the lattice in an extended system reduces the strength of electron-electron repulsion, making them easier to account for with an exchangelike kernel, and therefore RPAr tends to converge to 1 meV error or less between third and sixth order. Further development and implementation of spin-dependent kernels, such as the NEO kernel, are needed in order to better understand the difficulty that RPAr faces when combined with spin-dependent kernels.

For the spin-dependent rAPBE kernel on the left in Fig. 3, other than nitrogen, the first-row $2p$ elements converge extremely slowly. Boron and oxygen require a 12th-order approximation to drop below 5 meV error, while carbon still exhibits a residual error of approximately 40 meV at the same order. Using a linear fit from the log of the errors for RPAr6 through RPAr12 indicates that carbon requires approximately 32 orders to reach 1 meV error. This extremely slow convergence for these spin-polarized systems with the spin-dependent rAPBE kernel likely stems from the incomplete cancellation of the exchange and Coulomb interactions when they are treated independently [46]. Nitrogen avoids this issue and converges as rapidly as the closed-shell systems. Since the spin density of a half-filled shell is spherical and similar to the total density of a closed-shell system, the underlying rAPBE kernel is less sensitive to the distinction. For the antiferromagnetic ground state of NiO and the ferromagnetic ground states of Fe-bcc and the (0001) surface of cobalt, the convergence is similar to nitrogen and the spin-unpolarized systems of Fig. 2, with errors on the order of 1 meV between fifth and sixth order in the expansion.

For these same spin-polarized systems, using the spin-independent kernel (rAPBEns) results in similar convergence to the spin-unpolarized systems in Fig. 2. As with the spin-dependent kernel, B, C, and O converge more slowly than the other systems, however, errors below 1 meV are still attained between third and sixth order of RPAr. This remarkable contrast in the convergence behaviors for these two kernels emphasizes the important fact that the choice of the exchange-correlation kernel can make a significant impact in the convergence behavior in real systems, just as it did for the low-density limit of the homogeneous electron gas, but that for systems other than atoms Eq. (11) does tend to converge rapidly.

So far we have presented results for systems near their equilibrium geometries, for which the RPAr convergence is reasonably smooth and rapid for both an exchangelike and exchange-correlation kernel. Away from equilibrium, low-order perturbation theory can diverge if the Kohn-Sham gap goes to zero as it does, for instance, in the dissociation of homonuclear diatomics. Figure 4 illustrates the convergence behavior of RPA renormalization (left) for four stretched bond lengths of dinitrogen ($R_{eq} = 110$ pm), as well as demonstrates the different magnitudes of each order in the RPAr expansion (right). RPAr converges rapidly near equilibrium as expected, but as the bond length increases the convergence slows and terms up to eighth order are required to reach an error of $\sim$1 meV or less. From the right-hand plot, it is clear that RPAr1

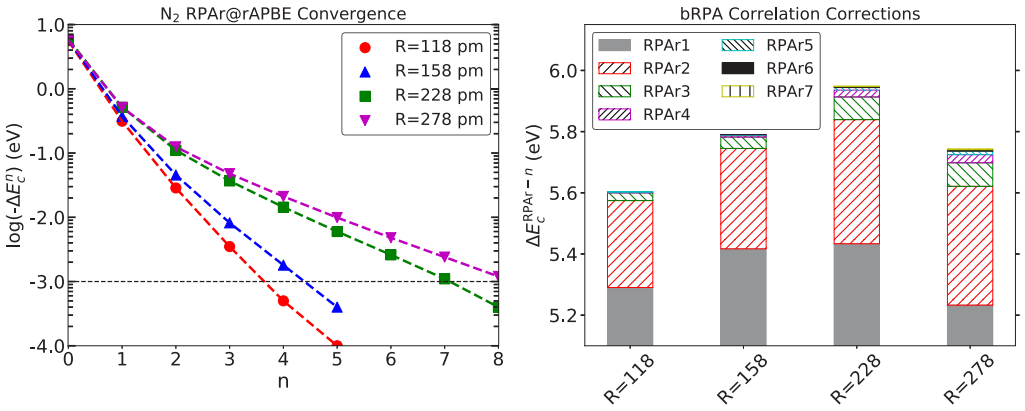

FIG. 4. Convergence (left) and bRPA correlation corrections (right) from RPAr for N_2 at four different stretched bond lengths with the rAPBE kernel. Near equilibrium ($R_{eq} = 110$ pm) RPAr is converged to less than 1 meV error by fourth order, however, convergence slows as R increases and terms up to eighth order or higher are required as the atoms dissociate. Still, even at double the equilibrium bond length, by fifth order RPAr is converged to approximately 10 meV error or less. Since RPA is the underlying approximation, the kernel corrections from RPAr remain finite even as the molecule dissociates and the Kohn-Sham gap goes to zero.

makes up the dominant contribution of the total beyond-RPA correlation energy, being on the order of 5.3 eV for all bond lengths. The contributions of second and higher orders amount to several hundred meV, with the second-order term dominating this beyond RPAr1 remainder. As the distance between the nuclei increases the relative contributions from higher orders increases which causes the convergence to be slower than at equilibrium, but no divergences are encountered even for bond lengths that are twice the equilibrium value and the series expansion still adds up to the infinite-order result. Even though higher-order terms are required at large separations, the contributions from fifth and higher orders amount to ∼10 meV, and can barely be discerned on the scale of the lower-order terms.

IV. DISCUSSION AND CONCLUSIONS

In order to accurately treat short-ranged correlation within the ACFD, an exchange-correlation kernel should be added to RPA. RPA renormalization provides a systematic route to compute such corrections, with the added benefit that both RPA and beyond-RPA contributions to the correlation energy can be computed simultaneously. RPA renormalization to first order had previously been applied to solids and molecules, but the behavior of higher orders had yet to be explored. We demonstrated numerically that beyond first order, RPAr tends to converge to the infinite-order result for spin-unpolarized systems of any band type, be it a molecule, metal, semiconductor, or insulator. For the spin-dependent kernel we tested, open-shell atoms were the slowest to converge for RPA renormalization likely due to the introduction of a Hartree-type component in the xc kernel [46]. Still, open-shell extended systems and some open-shell molecules also showed rapid convergence and we consider this challenge for atomic systems to be an exceptional case. In practice, the RPAr series converges to within 5 meV or better of the infinite-order result by fourth order for many of the systems we examined here.

Just as Bohm and Pines [1] originally used canonical transformations to map the interacting electron problem to one where long- and short-ranged forces can be accounted for in a two-step procedure, RPA renormalization accomplishes the same task via a straightforward refactorization of the Dyson-type equation for the interacting density-density response function (8). RPA, as the first step in both approaches, covers the long-range interactions present in a given system. The residual short-ranged forces beyond RPA are represented by f_{xc} within RPAr and are naturally screened by the RPA response function (11). This screening is tied directly to the monotonic behavior rationalized based on the properties of the bRPA correlation potential discussed in Sec. II. RPA renormalization tends to converge at a slower rate when combined with spin-dependent kernels, though this may be a limitation of the particular kernel we tested and further exploration of other spin-dependent kernels is needed to resolve the issue. Overall, however, RPAr provides a systematic framework for approximating exchange-correlation effects in the ACFD-DFT beyond RPA.

We would like to remark on two other aspects of the results that are not central to the convergence behavior. First, looking at all of the convergence plots as a whole, it is apparent that the performance of the first-order approximation is very consistent with the infinite-order approach and yields a roughly equivalent relative error for all of the systems we investigated. This point can be best understood by comparing the distribution of beyond-RPA corrections at $n = 0$ for each plot and noting that the distribution of relative errors for $n = 1$ is very similar. This underlying systematic character was previously attributed to the complete dependence of the RPAr1 correlation energy correction on the RPA response function [39,45]. Consequently, it may be possible to design an approximate correction beyond RPAr1 that also behaves systematically and recovers the missing correlation not captured in the first-order expansion. The second point is, again, that in addition to monotonic and rapid convergence towards the infinite-order result, RPA renormalization enables the computation of RPA and a kernel correction simultaneously. Separate calculations for RPA and a kernel correction are no longer needed since a single calculation yields both once the xc kernel and RPA

response function have been computed. The utility of this aspect of RPAr has yet to be fully realized and we plan to leverage it in our future work.

ACKNOWLEDGMENTS

We thank H. Peng and M. Reuter for insightful discussions, and L. Constantin for providing us with a subroutine to evaluate the CP07 kernel. We also thank C. E. Patrick and K. S. Thygesen for practical advice on the GPAW software. A.R., J.E.B., and J.S. acknowledge NSF for financial support. The design of the work was supported by National Science Foundation under Grant No. DMR–1553022 and by the donors to the American Chemical Society Petroleum Research Fund under Grant No. 57003–DNI10. The work of A.R. for the surfaces was part of the Center for the Computational Design of Functional Layered Materials, an Energy Frontier Research Center (EFRC) funded by the US Department of Energy, Office of Science, Basic Energy Sciences, under Award No. DESC0012575. This work was also supported in part by the National Science Foundation through major research instrumentation Grant No. CNS–09–58854. Figures were created using MATPLOTLIB [90].

[1] D. Bohm and D. Pines, Phys. Rev. **85**, 338 (1952).
[2] D. C. Langreth and J. P. Perdew, Phys. Rev. B **15**, 2884 (1977).
[3] P. Hohenberg and W. Kohn, Phys. Rev. **136**, B864 (1964).
[4] W. Kohn and L. J. Sham, Phys. Rev. **140**, A1133 (1965).
[5] F. Furche, Phys. Rev. B **64**, 195120 (2001).
[6] F. Furche, J. Chem. Phys. **129**, 114105 (2008).
[7] J. F. Dobson, J. Wang, B. P. Dinte, K. McLennan, and H. M. Le, Int. J. Quantum Chem. **101**, 579 (2005).
[8] M. Fuchs, Y. M. Niquet, X. Gonze, and K. Burke, J. Chem. Phys. **122**, 094116 (2005).
[9] L. Schimka, J. Harl, A. Stroppa, A. Grüneis, M. Marsman, F. Mittendorfer, and G. Kresse, Nat. Mater. **9**, 741 (2010).
[10] S. Lebègue, J. Harl, T. Gould, J. G. Ángyán, G. Kresse, and J. F. Dobson, Phys. Rev. Lett. **105**, 196401 (2010).
[11] H. Eshuis and F. Furche, J. Phys. Chem. Lett. **2**, 983 (2011).
[12] T. Björkman, A. Gulans, A. V. Krasheninnikov, and R. M. Nieminen, Phys. Rev. Lett. **108**, 235502 (2012).
[13] H. Eshuis, J. E. Bates, and F. Furche, Theor. Chem. Acc. **131**, 1084 (2012).
[14] X. Ren, P. Rinke, C. Joas, and M. Scheffler, J. Mater. Sci. **47**, 7447 (2012).
[15] J. Paier, X. Ren, P. Rinke, G. Scuseria, A. Grüneis, G. Kresse, and M. Scheffler, New J. Phys. **14**, 043002 (2012).
[16] H. Peng and S. Lany, Phys. Rev. B **87**, 174113 (2013).
[17] L. Schimka, R. Gaudoin, J. Klimeš, M. Marsman, and G. Kresse, Phys. Rev. B **87**, 214102 (2013).
[18] A. M. Burow, J. E. Bates, F. Furche, and H. Eshuis, J. Chem. Theory Comput. **10**, 180 (2014).
[19] C. E. Patrick and K. S. Thygesen, J. Chem. Phys. **143**, 102802 (2015).
[20] C. Waitt, N. M. Ferrara, and H. Eshuis, J. Chem. Theory. Comput. **12**, 5350 (2016).
[21] C. E. Patrick and K. S. Thygesen, Phys. Rev. B **93**, 035133 (2016).
[22] J. E. Bates, P. D. Mezei, G. I. Csonka, J. Sun, and A. Ruzsinszky, J. Chem. Theory Comput. **13**, 100 (2017).
[23] H. Eshuis, J. Yarkony, and F. Furche, J. Chem. Phys. **132**, 234114 (2010).
[24] M. Del Ben, J. Hutter, and J. VandeVondele, J. Chem. Theory Comput. **9**, 2654 (2013).
[25] M. Kaltak, J. Klimeš, and G. Kresse, Phys. Rev. B **90**, 054115 (2014).
[26] M. Kállay, J. Chem. Phys. **142**, 204105 (2015).
[27] J. Wilhelm, P. Seewald, M. Del Ben, and J. Hutter, J. Chem. Theory Comput. **12**, 5851 (2016).
[28] H. Jiang and E. Engel, J. Chem. Phys. **127**, 184108 (2007).
[29] Z. Yan, J. P. Perdew, and S. Kurth, Phys. Rev. B **61**, 16430 (2000).
[30] F. Furche and T. Van Voorhis, J. Chem. Phys. **122**, 164106 (2005).
[31] T. Olsen and K. S. Thygesen, Phys. Rev. B **87**, 075111 (2013).
[32] J. Harl, L. Schimka, and G. Kresse, Phys. Rev. B **81**, 115126 (2010).
[33] A. Grüneis, M. Marsman, J. Harl, L. Schimka, and G. Kresse, J. Chem. Phys. **131**, 154115 (2009).
[34] M. Marsman, A. Grüneis, J. Paier, and G. Kresse, J. Chem. Phys. **130**, 184103 (2009).
[35] J. Toulouse, I. C. Gerber, G. Jansen, A. Savin, and J. G. Ángyán, Phys. Rev. Lett. **102**, 096404 (2009).
[36] J. Toulouse, W. Zhu, J. G. Ángyán, and A. Savin, Phys. Rev. A **82**, 032502 (2010).
[37] T. Gould and J. F. Dobson, Phys. Rev. A **85**, 062504 (2012).
[38] X. Ren, P. Rinke, G. E. Scuseria, and M. Scheffler, Phys. Rev. B **88**, 035120 (2013).
[39] J. E. Bates and F. Furche, J. Chem. Phys. **139**, 171103 (2013).
[40] J. F. Dobson and J. Wang, Phys. Rev. B **62**, 10038 (2000).
[41] L. A. Constantin and J. M. Pitarke, Phys. Rev. B **75**, 245127 (2007).
[42] T. Olsen and K. S. Thygesen, Phys. Rev. B **86**, 081103(R) (2012).
[43] D. Lu, J. Chem. Phys. **140**, 18A520 (2014).
[44] T. Olsen and K. S. Thygesen, Phys. Rev. Lett. **112**, 203001 (2014).
[45] J. E. Bates, S. Laricchia, and A. Ruzsinszky, Phys. Rev. B **93**, 045119 (2016).
[46] T. Olsen and K. S. Thygesen, Phys. Rev. B **88**, 115131 (2013).
[47] E. K. U. Gross and W. Kohn, Phys. Rev. Lett. **55**, 2850 (1985).
[48] M. Petersilka, U. J. Gossmann, and E. K. U. Gross, Phys. Rev. Lett. **76**, 1212 (1996).
[49] W. G. Aulbur, L. Jönsson, and J. W. Wilkins, Phys. Rev. B **54**, 8540 (1996).
[50] P. Ghosez, X. Gonze, and R. W. Godby, Phys. Rev. B **56**, 12811 (1997).
[51] N. S. Ostlund, J. Chem. Phys. **57**, 2994 (1972).
[52] P. Jorgensen, Annu. Rev. Phys. Chem. **26**, 359 (1975).
[53] N. J. Russ, T. D. Crawford, and G. S. Tschumper, J. Chem. Phys. **120**, 7298 (2004).
[54] W. Klopper, A. M. Teale, S. Coriani, T. Pedersen, and T. Helgaker, Chem. Phys. Lett. **510**, 147 (2011).
[55] A. Hesselmann and A. Görling, Phys. Rev. Lett. **106**, 093001 (2011).

[56] N. Colonna, M. Hellgren, and S. de Gironcoli, Phys. Rev. B **90**, 125150 (2014).
[57] K. Burke, M. Ernzerhof, and J. P. Perdew, Chem. Phys. Lett. **265**, 115 (1997).
[58] D. Frydel, W. M. Terilla, and K. Burke, J. Chem. Phys. **112**, 5292 (2000).
[59] A. M. Teale, S. Coriani, and T. Helgaker, J. Chem. Phys. **132**, 164115 (2010).
[60] A. Heßelmann and A. Görling, Mol. Phys. **109**, 2473 (2011).
[61] M. Lein, E. K. U. Gross, and J. P. Perdew, Phys. Rev. B **61**, 13431 (2000).
[62] J. Harl and G. Kresse, Phys. Rev. B **77**, 045136 (2008).
[63] J. P. Perdew and K. Schmidt, in *Density Functional Theory and Its Application to Materials*, Vol. 577, edited by V. Van Doren, C. Van Alsenoy, and P. Geerlings (AIP, New York, 2001), pp. 1–20.
[64] J. P. Perdew, K. Burke, and M. Ernzerhof, Phys. Rev. Lett. **77**, 3865 (1996).
[65] J. Tao, J. P. Perdew, V. N. Staroverov, and G. E. Scuseria, Phys. Rev. Lett. **91**, 146401 (2003).
[66] B. G. Janesko and G. E. Scuseria, J. Chem. Phys. **131**, 154106 (2009).
[67] A. L. Fetter and J. D. Walecka, *Quantum Theory of Many-Particle Systems* (Dover, New York, 2003).
[68] A. Grüneis, M. Marsman, and G. Kresse, J. Chem. Phys. **133**, 074107 (2010).
[69] L. Hedin, Phys. Rev. **139**, A796 (1965).
[70] W. D. Laidig, G. Fitzgerald, and R. J. Bartlett, Chem. Phys. Lett. **113**, 151 (1985).
[71] D. Cremer and Z. He, J. Phys. Chem. **100**, 6173 (1996).
[72] M. Seidl, J. P. Perdew, and S. Kurth, Phys. Rev. Lett. **84**, 5070 (2000).
[73] F. Manby and P. J. Knowles, J. Chem. Phys. **112**, 7002 (2000).
[74] R. F. Rinehart, Am. Math. Mon. **67**, 157 (1960).
[75] A. Heßelmann, J. Chem. Phys. **134**, 204107 (2011).
[76] A. Heßelmann and A. Görling, Mol. Phys. **108**, 359 (2010).
[77] T. S. Jauho, T. Olsen, T. Bligaard, and K. S. Thygesen, Phys. Rev. B **92**, 115140 (2015).
[78] A. Jain, S. P. Ong, G. Hautier, W. Chen, W. D. Richards, S. Dacek, S. Cholia, D. Gunter, D. Skinner, G. Ceder, and K. A. Persson, APL Mater. **1**, 011002 (2013).
[79] M. Walter, H. Häkkinen, L. Lehtovaara, M. Puska, J. Enkovaara, C. Rostgaard, and J. J. Mortensen, J. Chem. Phys. **128**, 244101 (2008).
[80] J. J. Mortensen, L. B. Hansen, and K. W. Jacobsen, Phys. Rev. B **71**, 035109 (2005).
[81] S. R. Bahn and K. W. Jacobsen, Comput. Sci. Eng. **4**, 56 (2002).
[82] P. E. Trevisanutto, A. Terentjevs, L. A. Constantin, V. Olevano, and F. D. Sala, Phys. Rev. B **87**, 205143 (2013).
[83] See Supplemental Material at http://link.aps.org/supplemental/10.1103/PhysRevB.95.195158 for a compressed file containing raw data, as well as a pdf describing the contents of the compressed file and computational details.
[84] P. E. Blöchl, Phys. Rev. B **50**, 17953 (1994).
[85] H. J. Monkhorst and J. D. Pack, Phys. Rev. B **13**, 5188 (1976).
[86] J. Yan, J. J. Mortensen, K. W. Jacobsen, and K. S. Thygesen, Phys. Rev. B **83**, 245122 (2011).
[87] R. Sundararaman and T. A. Arias, Phys. Rev. B **87**, 165122 (2013).
[88] L. Onsager, L. Mittag, and M. J. Stephen, Ann. Phys. (Leipzig) **473**, 71 (1966).
[89] A. Ruzsinszky, J. P. Perdew, and G. I. Csonka, J. Chem. Theory Comput. **6**, 127 (2010).
[90] J. D. Hunter, Comput. Sci. Eng. **9**, 90 (2007).